Synthesis of surfactant free SnS nanorods by solvothermal route with better electrochemical properties towards supercapacitor application

Himani Chauhan,[a] Manoj K Singh,[b] Safir Ahmad Hashmi,[b] Sasanka, Deka*[a]

[a]Department of Chemistry, University of Delhi, North campus, Delhi-110007, India

[b]Department of Physics, University of Delhi, North campus, Delhi-110007, India

Email: sdeka@chemistry.du.ac.in, ssdeka@gmail.com

Abstract: We demonstrate a simple, low cost, eco-friendly synthesis of surfactant free tin monosulfide (SnS) nanorods by solvothermal route for the application in supercapacitor devices with high specific capacitance. The as-synthesized SnS nanorods consisting intrinsic layered structure were thoroughly characterised by XRD, TEM, HRTEM, SEM, EDAX and BET techniques for understanding crystal structure, size, morphology and surface area. To explore potential applications for supercapacitor, the nanocrystals were fabricated into two electrode system without adding any binder, large area support or a conductive filler, and characterised by cyclic voltammograms, galvanostatic charge–discharge and electrochemical impedance spectroscopy measurements in aqueous 2 M Na_2SO_4 electrolyte. These SnS nanorods exhibit enhanced supercapacitor performance with specific capacitance, energy density and power density values of ~70 F g^{-1}, 1.49 Wh kg^{-1} and 248.33 W kg^{-1} respectively, which are found even two times higher than SnS-carbon composite and hence makes them a better alternative source for energy storage devices.
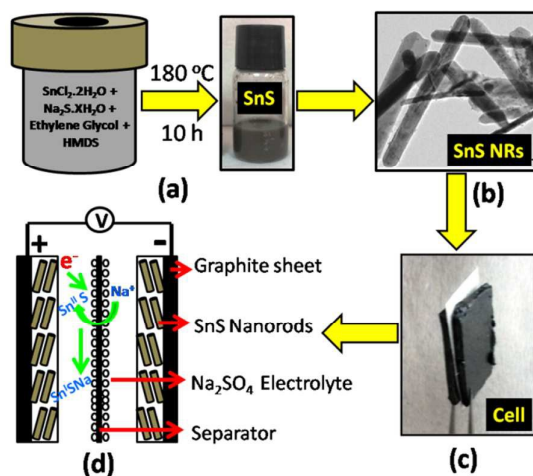
Keywords: SnS; nanorods; supercapacitor; pseudocapacitance; specific capacitance

1. Introduction

Supercapacitors, a family of electrochemical capacitors have been considered as one of the most promising energy-storage devices because of their many advantages, including faster charge/discharge processes, high power density, long cycle life and relatively low cost [1-4]. Pseudocapacitors, which along with electric double layer capacitors (EDLCs) create a supercapacitor store charge using redox-based Faradic reactions [5-8], thus can have higher capacitance values than electric EDLCs and can have higher power densities than that of secondary batteries. In the recent trend the specific capacitance values of pseudocapacitors have been tried to enhance by the use of emerging field of nanoscience and nanotechnology. Different allotropes of carbon [9,10], metal oxide and chalcogenide nanoparticles [11-13] or

their nanocomposites [14,15] have been explored as potential material for pseudocapacitors. In these cases for faradaic energy storage fast redox reactions makes charging and discharging much faster than batteries mainly due to preferred crystal structure, large area support and/or conductive filler. However, Sn- based chalcogenides, such as SnS, SnSe, SnS_2 and $SnSe_2$ which may be termed as multifunctional material due to their potential applications have not been widely investigated as supercapacitor (pseudocapacitor) material, but those were extensively used as anodic material for lithium ion batteries due to large volume expansions of these layered materials, as light absorber in solar cell, photodetector and as photocatalyst [16-21].

Among various tin chalcogenides, tin monosulfide (SnS) is important from electrochemical lithium ion storage as well as photovoltaic point of view. Tin monosulfide, also called herzenbergite, was first reported by the German mineralogist R. Herzenberg, and exists in GeS crystal form possessing each Sn atom coordinated by six S atoms results in distorted octahedral geometry of system [22]. SnS poses two layers per unit cell with one long distance S between the neighbouring layers. This type of layer structure is of particular interest owing to the arrangement of the cations and anions within the structural lattice where the layers of cations are separated by weak van der Waals forces. This layer structure of tin sulphides facilitates the intercalation of ions (Na^{+1}, Li^{+1} etc.) and makes them more favourable alternative with an improved electrochemical performance as anodic material. Bulk SnS has indirect 1–1.2 eV and direct optical band gap of 1.2–1.5 eV, a high solar conversion efficiency and a high absorption coefficient $\alpha > 10^4$ cm^{-1} [23]. Particularly, high absorption coefficient, dual carrier nature (p-type and n-type), low-cost and non-toxicity have made it a promising candidate for potential applications. There are few reports in recent years on the size and shape controlled synthesis of SnS nanostructures, for instance narrow size quantum dots, nanorods, ultrathin nanoribbons and nanosheets [23-26,18] and their unusual optical, electronic, and mechanical properties have been investigated extensively. To the best of our knowledge, there are only few reports where SnS has been introduced as a new electrode material for electrochemical capacitors, however making a nanocomposite with high surface area carbon powder [27,28] and with lower specific capacitance.

Scheme 1. Schematic view of synthesis, as-obtained particles and device fabrication (two electrode system) for Tin monosulphide NRs.

In this report for the first time we are introducing SnS nanorods (NRs) as a supercapacitor (pseudocapacitor) material synthesized by a simple, low cost and eco-friendly solvothermal method which is quite novel in tin sulphides chemistry. We synthesised surfactant free (without the use of any surfactant or stabilizing agent) NRs like morphology of SnS nanoparticles by solvothermal approach as shown in scheme 1 in ethylene glycol (EG) solvent, at 180° C for 10 hr in presence of HMDS as shape moderator [19]. Stannous chloride and sodium sulphide first react in EG to give smaller SnS particles due to the adsorption of polar EG solvent molecules on their surface [29-30]. In the present case, however addition of shape moderator HMDS directs the growth of the particles in an anisotropic way in 1D leading to nanorod morphology. The high surface area and the two-dimensional layered characteristics of these lamellar as-synthesized SnS NRs are advantageous to alkali metal intercalation phenomena; and hence can be proposed as good energy storage device due to high exchange of ions at the interface [31]. As shown in scheme 1c,d, a two electrode cell has been developed without the addition of any binder, large area support and/or conductive filler and high value of specific capacitance, energy density and power density of ~70 Fg^{-1}, 1.49 Wh kg^{-1} and 248.33 W kg^{-1}, respectively, has been demonstrated as a first case for SnS NRs using cyclic voltammogram , electrochemical impedance spectroscopy and charge-discharge studies. These parameters are accountably higher than the previous reports on SnS nanoparticles and their respective carbon composites [27-28].

2. Experimental details

2.1 Materials: Stannous chloride ($SnCl_2.2H_2O$, SRL-India, 99%), sodium sulfide ($Na_2S.xH_2O$, Thomas baker-India, 85%), hexamethyldisilazane (HMDS, Sigma Aldrich-USA, 99%), ethylene glycol (EG, SRL-India, 99%). All the chemicals were used without any further purification.

2.2 Synthesis of SnS NRs: In a typical synthesis process, 1mmol of $SnCl_2.2H_2O$ was dissolved in minimum amount of water and then 20 mL of EG and 2 mL of HMDS were added to it and stirred for 30 min. Another well stirred solution of 5 mmol sodium sulphide (dissolved in minimum amount of water) and 20 mL EG was added to the above solution drop-wise and stirred for another 30 min. This reaction mixture was transferred to a 50 mL Teflon-lined stainless steel hydrothermal vessel and the vessel was sealed and maintained at 180 $^{\circ}$C for 10 h. On completing the reaction the as-obtained black product was washed and finally dispersed in 1 mL of ethanol to treat as stock solution for further characterization and study.

2.3 Instrumentation: Powder X-Ray Diffraction (XRD) patterns of the as-synthesized products were collected at room temperature using a Bruker D8 Advance diffractometer system employing monochromatized Cu Kα radiation (λ = 1.54056 Å) source. Concentrated nanocrystal solutions were spread on top of a glass substrate, after which the sample was allowed to dry and then measured in reflection geometry. Data were collected at a fixed incident angle of about 1°. Optical absorption measurements were carried out using a Perkin Elmer Lamda 35 UV-Visible spectrophotometer. A diluted, well dispersed solution of NRs in absolute ethanol was used for absorption study. Transmission electron microscopy (TEM) and phase-contrast high resolution TEM (HRTEM) measurements were performed with a FEI Technai G^2-20 transmission electron microscope operating at an accelerating voltage of 200 kV. Samples suitable for TEM observation were prepared by applying one drop of dilute SnS NRs dispersion in ethanol onto the carbon coated Cu grid and allowing the solvent to slowly evaporate at room temperature. Scanning electron microscopy (SEM) and electron diffraction for X-ray analysis (EDAX) measurements were performed with a JEOL JSM 6610 at 20 kV, width distance 10 mm and spot size 30. EDAX was performed at a resolution of 135.2 eV. For SEM/EDAX measurements, a dilute and well dispersed solution of SnS NRs in ethanol was spread on top of 1cm x 1cm glass substrate and dried at room temperature.

2.4 Electrochemical Analysis: In order to prepare electrodes for supercapacitors, a dilute and well sonicated dispersion of SnS in ethanol was spin coated on graphite sheets (250 µm

thick, Nickunj.Eximp.Entp. India) and dried in oven at ~50 ºC overnight. The area of cell assembly was ~1 cm^2 and weight of electrode material (1.5 mg/cm^{-2}) deposited on graphite sheet was determined by weighing the graphite sheet before and after the spin coating of the electrode material. An aqueous solution of 2M Na_2SO_4 was used as electrolyte for device making as shown in scheme-1 (panel-d) and two-electrode geometry was chosen for the characterization of the capacitor cells. The two electrode super/pseudo-capacitor cell configurations using SnS NRs as electrode material (without binder) and 2M Na_2SO_4 as electrolyte is schematically given as follows:

<div align="center">Cell: SnS$_{NRs}$ // SnS$_{NRs}$</div>

The electrochemical characterization of capacitor cells was performed by cyclic voltammetry (CV), galvanostatic charge-discharge tests and electrochemical impedance spectroscopy (EIS). The CV and EIS responses were recorded with the electrochemical analyzer (660E, CH Instruments, USA) and the charge-discharge tests were performed at constant current using a charge-discharge unit (BT-2000, Arbin Instruments, USA).

3. Results and Discussion

The powder XRD pattern of the as-synthesised sample was refined for its crystal structure and found well indexed with herzenbergite SnS structure with an orthorhombic (pseudo-tetragonal distorted NaCl) unit cell (a = 4.329 Å, b = 11.190 Å, c = 3.983 Å; JCPDS No:39-0354, space group: D_{2h}:$Pnma$) without presence of any other impurity. The powder XRD pattern of the sample is compared with the bulk XRD pattern of herzenbergite SnS in Figure 1. No other phase of Sn-S (such as Sn_2S_3 and SnS_2) from their phase diagram [32] was found in the XRD pattern. The only detected effect which can be ascribed to the huge increase in intensity of 040 peak with respect to 111 peak (see inset of Figure 1a). The interesting fact obtained in the XRD pattern of the as-synthesized SnS is that the peak intensity ratio of (040)/ (111) planes was higher than that of bulk SnS. The peak intensity ratio of (040)/ (111) in bulk SnS is 0.66, where as the observed ratio for our SnS sample is 1.18. The vertical stretching in the peak intensity can be explained by a bigger domain of the SnS particles along the 040 direction with respect to the bulk sample. These preliminary results suggests a better exposure of the (040) surfaces relative to (111) surface in the present SnS NRs as compared to the bulk SnS particles and plausible growth of the expected NRs in <040> direction.
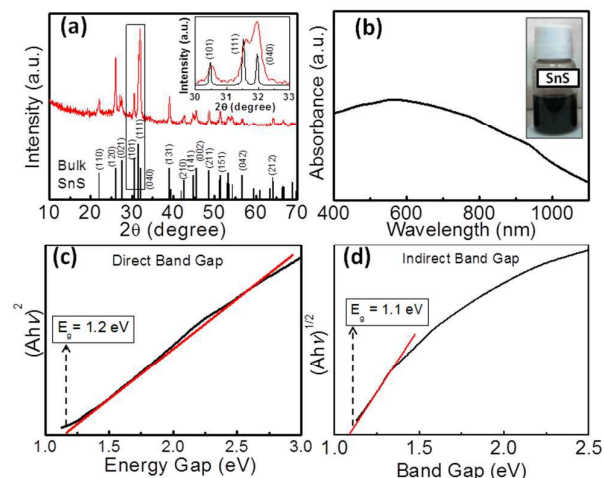
Figure 1. (a) Comparison of XRD pattern of as-synthesised SnS NRs (red curve) with bulk orthorhombic herzenbergite SnS (black curve). (b) Optical absorption spectrum of as-synthesized SnS NRs in ethanol dispersion (inset: dispersed solution), (c, d) determination of direct and indirect band gap, respectively following Tauc and Davis-Mott model.

Since a true optical band gap is an indication of a pure phase of a material, we have performed the optical absorption measurements and determined the band gap of our as-synthesized SnS NRs and results are shown in Figure 1b-d. To determine the optical band gap Tauc and Davis-Mott model was followed.

$$(\alpha h\nu)^n = A^*(h\nu - E_g) \qquad (1)$$

where $h\nu$ is the photon energy, n is an index characterizing the type of optical transition, A^* is a certain frequency independent constant, E_g is optical band gap and α is absorption coefficient defined by Beer-Lambert law as follows

$$\alpha = -\ln A/l \qquad (2)$$

where A is the absorbance and l is optical path length. To determine optical band gap and the nature of transition, we plot $(Ah\nu)^n$ vs. $h\nu$, where $n = 2$ for direct transition and $n = \frac{1}{2}$ for indirect transition. Linear part near the absorption edge was observed for both the transitions, i.e. for $n = 2$, and $n = \frac{1}{2}$ as shown in Figure 1c, d respectively, depicting the presence of direct and indirect band gap of the as-synthesized SnS NRs. A direct band gap value of 1.20 eV is determined from the extrapolated intercept with the Energy ($h\nu$) axis (Figure1c). On the other hand, indirect inter-band transitions gap of 1.1 eV was determined from Figure 1d. Both the direct and indirect band gap values are consistent with earlier reports for SnS samples [33], depicting a pure phase of our as-synthesized SnS NRs. However, we have not observed predicted blue shift in band gap, might be due to larger size of the particles.

Morphology, topology and crystal structure of the as-synthesized samples have been investigated by TEM and HRTEM, and the images are summarized in Figure 2. The low magnified TEM images at scale of 500 nm, 100 nm and 50 nm respectively in panel a-c from different grid area show the anisotropic 1D nature of the SnS. All as-obtained particles are found to be nanorod in morphology, however with large particle size distribution. On plotting histogram for the length and diameter separately (Figure 2d, e), the average dimension of SnS NRs is found to be 60 nm × 450 nm. This observed wide distribution of particle size or the polydispersity is related to the surfactant free synthesis condition of the NRs, where absence of any surface or facet selective surfactant leads the growth of the NRs unhindered. However with the help of HRTEM analyses, we tried to understand the NRs preferential growth direction and the reason behind that. The lattice-resolved HRTEM image in Figure 2f shows inter planar spacing of 0.40 and 0.29 nm for the adjacent (110) and (040) planes of SnS, depicting the its pure orthorhombic phase. Further the fast fourier transform (2D-FFT, zone axis [0,0,4]) has been calculated from the HRTEM image and shown in Figure 2g. The clear spots in FFT also correspond to (110) and (040) planes corroborating the interlamellar spacing of 0.40 and 0.28 nm, respectively. As shown in the depiction of the planner crystal structure of SnS and the (110) and (040) planes seen under [0,0,4] zone axis; and the data obtained from HRTEM analyses, it could be clearly reasoned that the growth of the SnS nuclei after their formation in the solvothermal process takes place in <110> and <040> directions. Since the synthesis does not contain any surfactant, at 180 ^{o}C probably the growth favours thermodynamically in the said two directions and results in wide distribution of particles. In addition the experimental results suggest a dihedral angle between these two sets of fringes is 46°, which match well with the angle between Miller planes i.e. 45° as shown in Figure 2f, h. Topography and elemental composition were further analysed with SEM and EDAX and shown in Figure 3. Clear view of NRs seen under SEM imaging with similar dimensions as established from TEM measurements. A single nanorod of SnS was chosen for elemental analysis on line alignment along the length (inset of panel a), which gives Sn:S ratio of nearly 1:1 within the instrumental error.
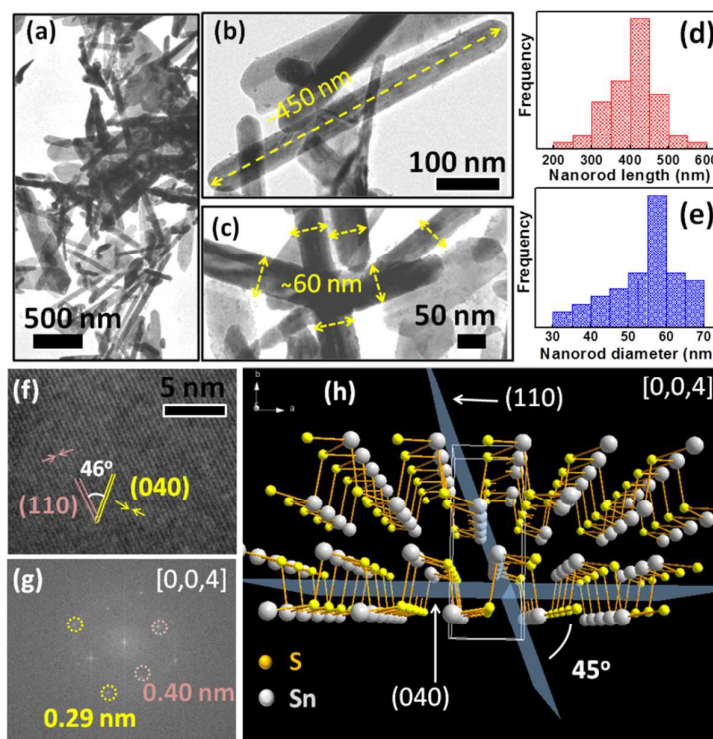
Figure 2. Characterization of SnS NRs. (a-c) Low magnified TEM images at different scale, (d,e) particle size distribution of the as-synthesized SnS NRs in lateral and longitudinal directions, (f) HRTEM image showing lattice fringes belong to (110) and (040) planes, (g) calculated 2D-FFT pattern from panel 'f' and (h) Depiction of the layer crystal structure of SnS seen from [0,0,4] zone axis.
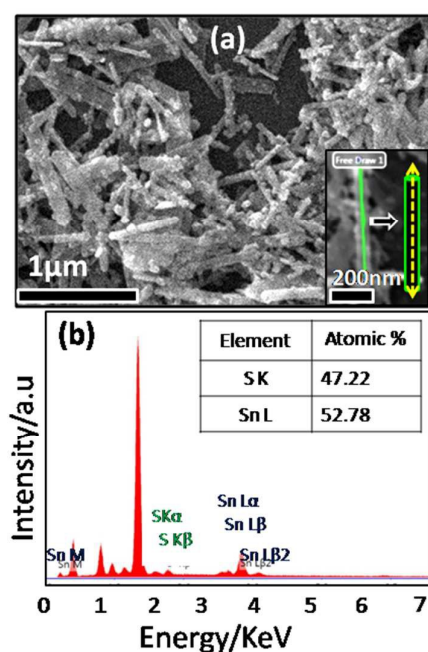
Figure 3. (a) SEM image of as-synthesized sample showing a 3-dimensional view of SnS NRs, inset: SEM image of single SnS nanorod taken for EDAX and (b) EDAX spectrum from elemental analysis.

Surface area study: A high value of surface area of nanoparticles (surface area >10 m^2/g) makes them suitable as better supercapacitor electrodes [34] In view of this, the specific surface area of SnS NRs was determined from the Brunauer–Emmett–Teller (BET) plots (not shown) using the multipoint BET equation. A high value of specific surface area (~221 m^2/g) has been obtained for SnS NRs, observed under repeated measurements on different batches of samples. The N_2 adsorption-desorption measurement indicates the porous texture of the as-synthesised SnS NRs, as shown in Figure 4, which is referred as Type-IV isotherm with H3-type hysteresis according to IUPAC classification. The predominant mesoporosity in the material could be indicated from the slowly increasing isotherm and the hysteresis loop. The sudden jump at around 3 nm and broad pore size distribution between 15 to 25 nm (inset of Figure 4) indicates that two different sized mesopores are present in SnS NRs. The mesopore volume is estimated from the isotherm and found to be ~ 0.26 cm^3 g^{-1}. The H3-type hysteresis loop indicates that the material basically contains slit-shaped pores at SnS nanorod surface. Particularly, the nanostructured tin sulphides with controlled morphologies possess larger surface area, greater accessibility to the electrolytes, faster transportation of ions, and accelerated phase transitions [35] due to it's intrinsic layer crystal structure. Thus, we can expect a large capacitance value due to the observed high surface area of as-synthesized layered SnS NRs. Chemically the origin of pseudocapacitance in electroactive material like SnS is mainly due to the intercalation redox reactions, which strongly depends on the particle size and morphology of nanoparticles [34]. Thus, larger number of intercalating anions between the layers of hergenbergite SnS is available for redox reactions, which is the origin of pseudocapacitance in the present case.
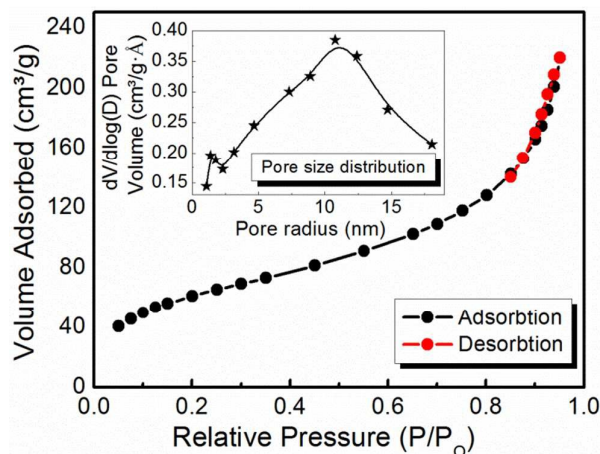
Figure 4. N_2 adsorption/desorption isotherm of SnS nanorod sample at 77 K. Inset: Pore volume distribution vs. pore radius of the as-synthesized nanorods.

Electrochemical study: The CV studies have been performed at different scan rates in symmetric potential window of -0.4V to +0.4V and also in the potential range of 0.1V to 1.0 V as used for galvanostatic charge-discharge cycling (presented later). Figure 5a,b depicts scan rate dependent voltammograms of the capacitor cell, which are close to rectangular shapes even at higher scan rates. This is an important characteristic of the supercapacitors indicating their high rate capability, i.e. fast charging and discharging of the devices. Further, the recyclability of the capacitor cells with the electrodes of as prepared tin sulfide nanoparticles has been tested by CV cycling at a scan rate of 50 mV s^{-1} in the potential window of 0.1 V to 1.0 V, as shown in Figure 5c. The test indicates the excellent stability of the SnS NRs as electrode material for many cycles.

In general, the capacitors, employing active redox electrodes like SnS (as in the present case), have the combined effect of double layer capacitance and the pseudocapacitance owing to the fast redox reactions at the electrode-electrolyte interfaces. In the present system, the possible reactions involved to obtain pseudocapacitive behavior at the SnS-nanorod electrode/electrolyte interface are [36]:

$$\text{Redox reaction: } Sn^{II}S \ + \ Na^+ \ \longleftrightarrow \ Sn^{I}SNa \ + \ e^- \qquad (3)$$

Or

$$SnS \ + \ 2Na^+ + \ 2e^- \ \longleftrightarrow \ Sn \ + \ Na_2S \qquad (4)$$

It may be noted that the CV patterns show almost rectangular shapes up to the scan rate of 50 mV s^{-1}, whereas the little deviation in the curves has been found at higher scan rate, which is primarily due to the resistive components of the cell. It may further be noted that the nanostructured tin sulphides i.e. SnS NRs possess high surface area than the bulk and moreover due to their unique layered structure, they have a potential to enhance the electrochemical performance as supercapacitor electrode material. The enhanced supercapacitive behaviour of SnS NRs over bulk SnS (discussed above) is mainly due to the intercalation of Na$^+$ ions into the van der waals gap of S-Sn-S layers. As the large surface area of these nanostructure tin sulphides greatly reduces the diffusion length over which both ions and electrons transfer takes place during the charge-discharge process, the better capacitance value is obtained on nanostructuring. This observation is also in agreement with the capacitance obtained for layered SnS nanostructures which shows better proper

compatibility and the formation of excellent capacitive interfaces with the SnS NRs electrode than bulk SnS electrode [27].
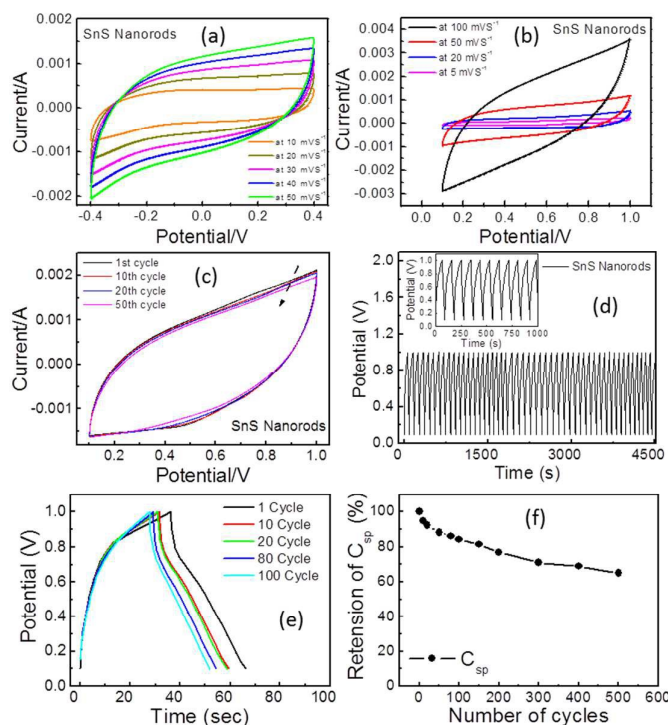

Figure 5. Cyclic voltammograms of Cell (a) CV in symmetric window of -0.4V to +0.4V at different scan rates, (b) CV in asymmetric potential window 0.1V to 1.0V, (c) CV for various number of cycles at scan rate of 50 mV s^{-1}, (d) Galvanostatic charge-discharge profile of Cell in potential range from 0.1 V to 1.0 V at the current of 0.5 mA cm^{-2} (inset few cycles), (e) comparison of charge-discharge profile for various cycles and (f) plot of capacitance vs number of cycles for cycling stability of SnS nanorod as supercapacitor material.

Figure 5d shows the charge-discharge characteristics of the capacitor cell in the potential range 0.1 to 1 V as CV, recorded at a constant current of 0.5 mAcm^{-2}. The characteristics of the cells are observed to show a capacitive nature as characterized by almost linear discharge patterns. The discharge capacitance has been evaluated from the discharge characteristic regions using the expression [6, 37]:

$$C_{cell} = \frac{i.\Delta t}{\Delta V} \qquad (5)$$

where i is the discharge current, and $\Delta t/\Delta V$ is the inverse of slope of discharge curve. The specific capacitance of electrode material is obtained by expression $C_{sp}=2*C_{cell}/m$, where m is the mass of the single electrode. The capacitance value for SnS NRs based cell has been evaluated from eq. 5 and found to be ~70 F g^{-1}, which is more or even twice than the reported

values of the capacitors based on electrodes of bulk SnS and even SnS-carbon nanocomposite [27,28]. As SnS NRs are of layered structure, the better capacitance behaviour is expected due to more encapsulation of Na^+ ions between the two layers of tin sulphide both orthogonal lattices of SnS. Charge-discharge profile shows a decrease in capacitance value as the number of cycle increases. The capacitance C_{sp} decreases as electrolyte ions block the pores of electrode materials as in the present case, the electrolyte ions Na^+ and SO_4^{-2} have the possibility to be trapped in to the layers of SnS NRs and they do not participate in further redox reactions.

Figure 5e depicts the galvanostatic charge−discharge behavior of the two electrode cell of SnS at different cycles (up to 100 cycles) in a potential window of 0 to +1 V. Figure 5f shows the variation of capacitance (C_{sp}) with cycles and it was found that up to 150 cycles capacitance value is reduced by 20% and the C_{sp} retains 60% of its initial value until 500 cycles. This observation might be possibly due to the blockage of mesoporos by SO_4^{-2} (from Na_2SO_4). The efforts are continued to improve the performance of capacitance by adding graphene or other carbon active material in future work.
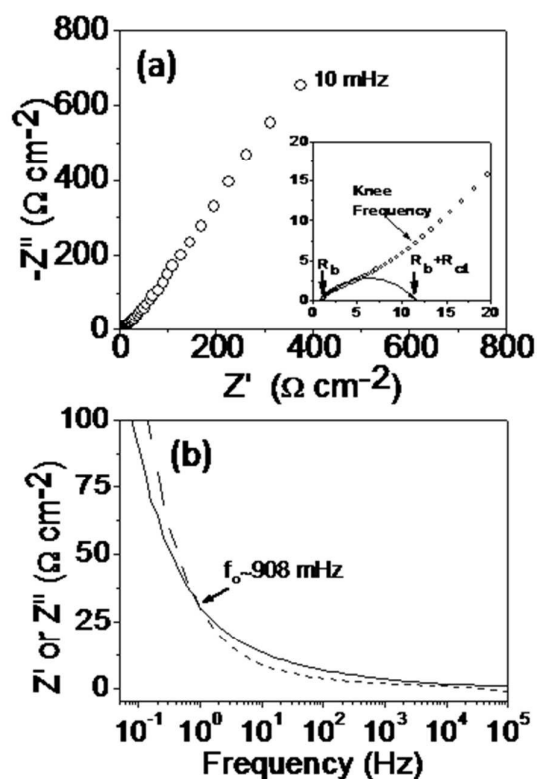
Figure 6. (a) EIS plot, recorded in the frequency range from 10 mHz to 100 kHz; the expanded representation of EIS plot in high to mid-frequency range shown in inset, and (b) Bode plots of the cell.

The other important parameters namely specific energy and power density have also been evaluated using the following expressions [38]:

$$E = \frac{1}{2M} C_{cell} V^2 \tag{6}$$

$$P = \frac{V^2}{4M * ESR} \tag{7}$$

Where C_{cell} is the capacitance of the cell (in Fcm^{-2}), V is the voltage excluding the equivalent series internal resistance (ESR) occurring at the beginning of the discharge profile of the cell, and M is the mass of the both the capacitor electrodes. The ESR value of the cell is observed to be ~ 215 Ωcm^2. The specific energy and power density of the capacitor cell have been evaluated to be ~ 1.5 Wh kg^{-1} and ~ 248 W kg^{-1}, respectively.

The EIS pattern i.e. the plot between real $(Z^{'})$ and imaginary part $(Z^{"})$ of the impedance (Z), of the SnS-nanorod-based capacitor cell is shown in Figure 6(a), indicating its capacitive behaviour as reflected by the steeply rising pattern in the lower frequency range [39]. This capacitive impedance response is accompanied with high-frequency semicircular feature showing mainly the bulk property of tin sulphide and the electrode-electrolyte interfaces, as shown in the expanded representation in the high frequency range (Figure 6a inset). A depressed semicircular arc has been drawn based on experimental points in the high frequency region (Figure 6a, inset). The arrows marked on the arc indicate the bulk electrolyte resistance R_b and $R_b+ R_{ct}$ (R_{ct} being charge-transfer resistance). The values of R_b, R_{ct} and the overall resistance at 10 mHz (R) has been found to be ~ 1.17, ~ 11.4 and ~ 375 Ω cm^2, respectively. Followed by semicircular arc, EIS plot shows a linear pattern with the slope of $\sim 45^{\circ}$ angle, beyond that the steeply rising capacitive pattern has been observed in low frequency region. The specific capacitance (C) has been evaluated from the expression C $= 2/ (2\pi f m Z^{"})$ (where m is the mass of the single SnS electrode, and $Z^{"}$ is imaginary part of impedance at frequency f) and found to be 30.3-34.7 F g^{-1} at the frequency 10 mHz. This value is lower than the specific capacitance observed from charge-discharge studies, discussed earlier.

The rate capability of the supercapacitor has also been evaluated in terms of knee frequency, and response time from the EIS studies [40]. Below knee frequency, the impedance pattern shows steeply rising capacitive response, whereas the response time (τ_o) is

reciprocal of a frequency f_o at which the imaginary and real part of impedance with respect to the applied frequency (Bode plots) are equal [41]. The knee frequency of present capacitor cell is found to be ~15.8 Hz (inset of Figure 6a). Figure 6b depicts the Bode plots of the supercapacitor, showing f_o at ~908 mHz and corresponding τ_o of ~1.10 sec. The values of τ_o and knee frequency indicate the high rate performance of the capacitor cell with nanostructured SnS electrodes.

4. Conclusion:

In this report we introduced enhance supercapacitor behaviour of bare (surfactant free) SnS NRs synthesized by simple, eco-friendly and low cost solvothermal method. The SnS NRs are found to be grown in <110> and <040> directions due the presence of shape moderator as well as thermodynamically favourable crystal structure. Better supercapacitor behaviour with capacitance of ~70 Fg^{-1} using two-electrode system for as synthesised bare SnS NRs was observed, which is found much more than reported SnS-carbon composites and hence can be applicable as promising pseudocapacitor material for energy storage devices.

Acknowledgements

References

[1]   A. S. Arico, P. Bruce, B. Scrosati, J. M. Tarascon and W. V. Schalkwijk, *Nature Mater.,* 2005, **4**, 366.

[2]   P. Simon and Y. Gogotsi, *Nature Mater.,* 2008, **7**, 845.

[3]   C. Liu, F. Li, L. P. Ma and H. M. Cheng, *Adv. Mater.,* 2010, **22,** E28.

[4]   G. Wang, L. Zhang and J. Zhang, *Chem. Soc. Rev.*, 2012, **41,** 797.

[5]   Y. M. Vol'fkovich and T. M. Serdyuk, *Russian J. Electrochem.,* 2002, **38,** 935.

[6]   K. Deori, S. K. Ujjain, R. K. Sharma and S. Deka, *ACS Appl. Mater., Interfaces,* 2013, **5,** 10665.

[7]   S. Faraji and F. N. Ani, *J. Power Sources,* 2014, **263,** 338.

[8]   V. Augustyn, P. Simon and B. Dunn, *Energy Environ. Sci,* 2014, **7,** 1597.

[9]   E. Frackowiak and F. Beguin, *Carbon,* 2001, **39,** 937.

[10] Y. Zhu, S. Murali, M. D Stoller, K. J. Ganesh, W. Cai, P. J. Ferreira, A. Pirkle, R. M. Wallace, K. A. Cychosz, M. Thommes, D. E. Su, A. Stach and R. S. Ruoff, *Science,* 2011, **332,** 1537.

[11] W. Wei, X. Cui, W. Chena and D. G. Ivey, *Chem. Soc. Rev.*, 2011, **40,** 1697.

[12] C. D. Lokhande, D. P. Dubal and O. S. Joo, *Curr. Appl. Phys.,* 2011, **11,** 255.

[13] K. Krishnamoorthy, G. K. Veerasubramani, A. N. Rao and S. J. Kim, *Mater. Res. Express,* 2014, **1,** 035006.

[14] X. Huang, X. Qi, F. Boey and H. Zhang, *Chem. Soc. Rev.,* 2012, **41,** 666.

[15] M. Zhi, C. Xiang, J. Li, M. Li and N. Wu, *Nanoscale*, 2013, **5,** 72.

[16] K.T. R. Reddy, N. K. Reddy, R.W. Miles, *Sol. Energy Mater. Sol. Cells,* 2006, **90,** 3041.

[17] Y. Li and H. Xie and J. Wang, *J Solid State Electrochem,* 2011, **15**, 1115.

[18] Y. Zhang, J. Lu, S. Shen, H. Xu and Q. Wang, *Chem. Commun.,* 2011, **47,** 5226.

[19] Z. Deng, D. Cao, J. He, S. Lin, S. M. Lindsay, and Y. Liu, *ACS Nano,* 2012, **6,** 6197.

[20] Q. Wu, L. Jiao, J. Du, J. Yang, L. Guo, Y. Liu, Y.Wang and H. Yuan, *J. Power Sources*, 2013, **239,** 89.

[21] J. Xia, G. Li, Y. Mao, Y. Li, P. Shen and L. Chen, *Cryst Eng Comm,* 2012, **14,** 4279.

[22] T. Jiang, and G. A. Ozin, *J. Mater. Chem.* 1998, **8,** 1099.

[23] S. G. Hickey, C. Waurisch, B. Rellinghaus, and A. Eychmuller, *J. Am. Chem. Soc.,* 2008, **130,** 14978.

[24] D. Ma, H. Zhou, J. Zhang and Y. Qian, *Mater. Chem. Phys.*, 2008, **111***,* 391.

[25] Y. Xu, N. A. Salim, C. W. Bumby and R. D. Tilley, *J. Am. Chem. Soc.,* 2009, **131,** 15990.

[26] J. Ning, K Men, G. Xiao, L. Wang, Q. Dai, B. Zou, B. Liua and G. Zoua, *Nanoscale*, 2010, **2,** 1699.

[27] M. Jayalakshmi, M. Mohan Rao and B.M. Choudary, *Electrochem. Commun.*, 2004, **6,** 1119.

[28] Y. Li, H. Xie and J. Tu, *Mater. Lett.,* 2009, **63,** 1785.

[29] S. Sohila , M. Rajalakshmi, C. Muthamizhchelvan, S. Kalavathi, C. Ghosh, R. Divakar , C.N. Venkiteswaran, N.G. Muralidharan, A.K. Arora and E. Mohandas, *Mater. Lett.,* 2011, **65,** 1148.

[30] Y. Zhu,Y. Chen , L. Liu, *J. Cryst. Growth,* 2011, **328,** 70.

[31] C. H. Lai, M. Y. Lu and L. J. Chen, *J. Mater. Chem*., 2012, **22,** 19.

[32] R. C. Sharma and Y. A. Chang, *Bull. Alloy Phase Diagrams*, 1986, **7,** 269.

[33] M. Parenteau and C. Carlone, *Phys. Rev. B,* **41,** 5227.

[34] S. K. Meher, P. Justin and G. R. Rao, 2011, *Nanoscale,* 1990, **3,** 683.

[35] J. Ma, D. Lei, X. Duan, Q. Li, T. Wang, A. Cao, Y. Maod and W. Zheng, *RSC Adv.,* 2012, **2,** 3615.

[36] K. Jost, G. Diona and Y. Gogotsi, *J. Mater. Chem. A,* 2014*,* **2,** 10776.

[37] F. Beguin and E. Frackowiak, *Supercapacitors: Materials, Systems and Applications,* Wiley-VCH Verlag GmbH & Co. KGaA, 2013*,* ISBN 9783-527-32883-3.

[38] B. E Conway, *Electrochemical Supercapacitors: Scientific Fundamentals and Technological Applications,* Springer US, 1999, DOI 10.1007/978-1-4757-3058-6.

[39] Y. Kumar, G. P. Pandey and S. A. Hashmi*, J. Phys. Chem. C,* 2012, **116,** 26118.

[40] M. K. Singh, Y. Kumar and S. A. Hashmi, *Nanotechnology,* 2013, **24**, 465704.

[41] J. R. Miller, *Proc. 8th International Seminar on Double Layer Capacitor and Similar Energy Storage Devices*, Deerfield Beach, Florida, December 7-9, 1998.